Optical anisotropy in laterally aligned W_6Te_6 nanowire bundles

Ryusuke Natsui[1,2], Nguyen Tuan Hung[3], Desman Perdamaian Gulo[4], Keana Rylie Pasoquen[4], Muhammad Shoufie Ukhtary[5], Hsiang-Lin Liu[4], Riichiro Saito[2,4,6]*, Yasumitsu Miyata[1,2]*

Affiliations

[1]*Research Center for Materials Nanoarchitectonics (MANA), National Institute for Materials Science (NIMS), Tsukuba 305-0044, Japan*

[2]*Department of Physics, Tokyo Metropolitan University, Hachioji 192-0397, Japan*

[3]*Department of Materials Science and Engineering, National Taiwan University, Taipei 10617, Taiwan*

[4]*Department of Physics, National Taiwan Normal University, Taipei 11677, Taiwan*

[5]*Research Center for Quantum Physics, National Research and Innovation Agency (BRIN), South Tangerang 15314, Indonesia*

[6]*Department of Physics, Tohoku University, Sendai 980-8578, Japan*

Authors to whom correspondence should be addressed: r.saito.*sendai@gmail.com*, miyata.yasumitsu@nims.go.jp

Abstract

We report optical anisotropy in laterally aligned bundles of metallic W_6Te_6 nanowires, grown on *a*-plane sapphire substrates by chemical vapor deposition. Mueller-matrix spectroscopic ellipsometry reveals strong directional dependence in absorption (dichroism) and refraction (birefringence) along and across the nanowire axis. These experimental observations are qualitatively supported by first-principles calculations and consideration of depolarization effects. Our findings establish W_6Te_6 as a model system for studying light-matter interactions in anisotropic metallic nanostructures and demonstrate its potential for polarization-sensitive photonic and optoelectronic applications.

Quasi-one-dimensional (quasi-1D) van der Waals (vdW) materials have recently emerged as promising systems for studying directionally dependent light–matter interactions.[1-5] Their crystal structures consist of atomic chains or nanowires weakly bound via vdW interactions, resulting in highly direction-dependent charge transport and optical responses. When macroscopically aligned, such nanowires enable the direct observation of anisotropic optical properties, including polarization-dependent absorption (dichroism) and refractive index (birefringence). While semiconducting quasi-1D systems such as $BaTiS_3$, TiS_3, ZrS_3 and fibrous red phosphorus have been studied in this context,[1-5] metallic quasi-1D compounds remain unexplored.

Transition metal monochalcogenides (TMMs), with the general formula M_6X_6 (M = Mo or W; X = S, Se, or Te), represent prototypical metallic quasi-1D systems. Various studies have investigated the growth, structural, electronic, and transport properties of these materials.[6-24] Notably, theoretical studies have predicted pronounced optical anisotropy in these systems,[19,21] highlighting the need for experimental validation. Recently, polarization-dependent Raman measurements have been performed on individual bundles of W_6Te_6 nanowires.[14,17] To further advance our understanding of this phenomenon, it is necessary to explore optical anisotropy including absorption using well-aligned TMM arrays. However, experimental studies on aligned TMMs remain limited due to challenges in synthesizing large-area, oriented thin films. Recent advances in chemical vapor deposition (CVD) have enabled the growth of wafer-scale, aligned bundles of TMM nanowires on sapphire substrates,[14,15] providing a suitable platform for anisotropic optical measurements.

To validate these predictions, we investigate the optical anisotropy of laterally aligned bundles of W_6Te_6 nanowires using Mueller-matrix spectroscopic ellipsometry. The samples were grown on *a*-plane sapphire substrates and characterized using Raman spectroscopy and atomic force microscopy (AFM). Ellipsometry measurements reveal strong directional dependence in both absorption and refraction along and across the nanowire axis. These experimental results are further analyzed through first-principles calculations with additional consideration of depolarization effects.

Figures 1a–c show structural models of a W_6Te_6 nanowire bundle. In the *ab* plane (Fig. 1b), two W_3Te_3 triangular units are stacked along the *c*-axis in opposite orientations. Within the unit cell of the bundle, which consists of two W_6Te_6 nanowires, the W_3Te_3 triangles are also

arranged in opposite directions in the *ab* plane. Aligned W_6Te_6 bundles were grown on *a*-plane sapphire substrates using CVD with Te and WO_3, as previously reported.[14-17] Details of the CVD growth parameters, including the precursor, carrier gas flow, and growth time, are described in the Supplementary Material. The atomic arrangement and composition were confirmed by scanning transmission electron microscopy and energy-dispersive X-ray spectroscopy, respectively, in our previous study.[14,17]

Figures 1d,e and S1 display optical and AFM images of the aligned bundles, respectively. The bundles have a wide range of height, reaching up to ~10 nm. Considering the surface coverage of approximately 80% and the observed height distribution, the sample is approximated as a uniform thin film with a thickness of 5 nm. This value was used in the analysis of the spectroscopic ellipsometry data. The bright spots observed in Fig 1d are attributed to by-products, likely Te- and W-containing compounds. In the Raman spectrum (Fig. 1f), two prominent peaks at 155 cm^{-1} and 196 cm^{-1} correspond to the radial breathing mode of Te and W triangular clusters in the W_6Te_6 unit cell, respectively.[17] In addition, we note that the small peaks observed around 100 cm^{-1} are considered to originate from the nanowires because they exhibit a polarization dependence similar to that of the other Raman peaks assigned to W_6Te_6. Mueller-matrix spectroscopic ellipsometry[25] is performed using the configuration shown in Fig. 1g. Details of characterization, ellipsometry measurements/analysis, and theoretical calculations are provided in the supplementary material.

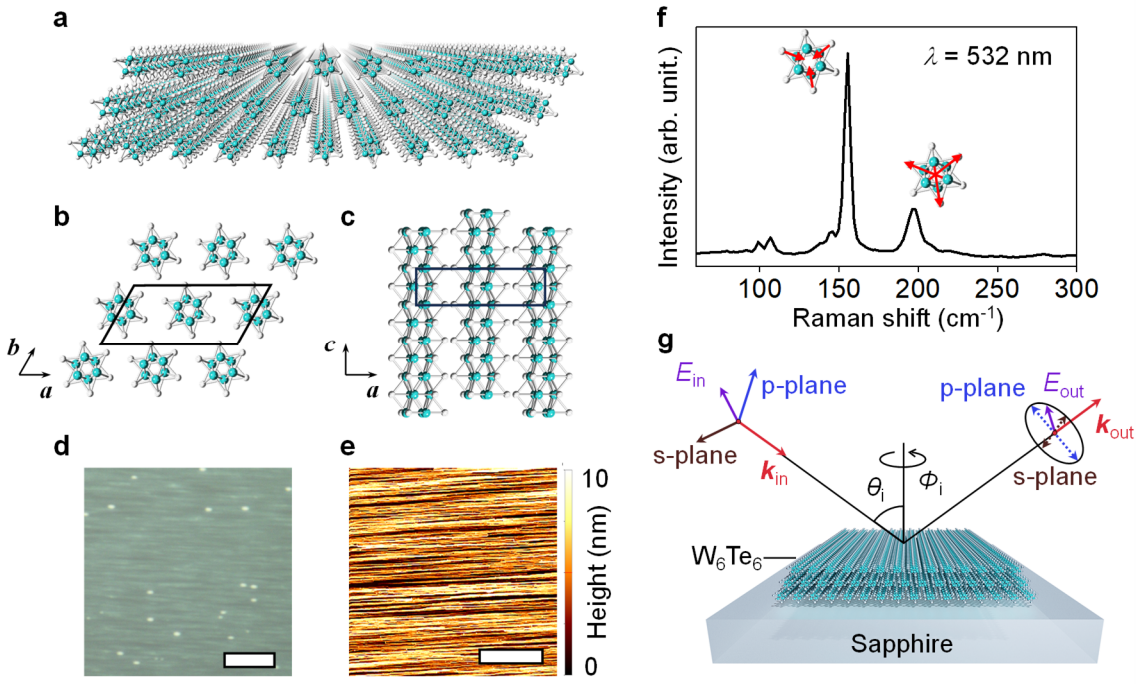

Figure 1. (a–c) Structural models of W_6Te_6 nanowires: (a) schematic illustration of a nanowire bundle, (b) cross-sectional view, and (c) side view of the atomic structure. Cyan and gray denote W and Te atoms, respectively. The unit cell is outlined with black boxes in the cross-sectional and side-view structures. The unit cell of the monoclinic phase is defined by the lattice parameters a=1.79 nm, b=0.91 nm, and an interaxial angle γ=58°.[17] (d) Optical and (e) AFM images of aligned W_6Te_6 bundles grown on an a-plane sapphire substrate. Scale bars: (d) 10 μm, (e) 3 μm. (f) Raman spectrum of aligned W_6Te_6 bundles measured using a 532 nm excitation laser. Schematic images next to the peaks show the eigenvectors of the corresponding Raman-active normal modes. (g) Schematic illustration of the experimental configuration used for spectroscopic ellipsometry measurements. The incident and reflected light vectors (k_{in}, k_{out}) define the angle of incidence (θ_i) and the azimuthal angle (Φ_i) with respect to the nanowire alignment direction. The electric field vectors (E_{in}, E_{out}) are decomposed into s- and p-polarized components relative to the plane of incidence.

Figure 2a shows the experimental absorption coefficient spectra of aligned W_6Te_6 bundles obtained from spectroscopic ellipsometry. The absorption coefficient in the parallel direction ($\alpha_\parallel$) is consistently higher than that in the perpendicular direction ($\alpha_\perp$) over the entire photon energy range. In particular, $\alpha_\parallel$ exhibits two distinct peaks near 2.4 eV and 3.3 eV. These

spectral features are qualitatively consistent with transmission spectra previously reported for thin films of randomly oriented W_6Te_6 nanowire bundles.[14] In contrast, $\alpha_\perp$ shows a more gradual increase with photon energy. At 3.5 eV, the value of $\alpha_\perp$ is approximately half that of $\alpha_\parallel$. Given that the sapphire substrate is optically isotropic (See details in the Supplementary Material), the observed anisotropy arises from the intrinsic absorption properties of the aligned W_6Te_6 bundles.

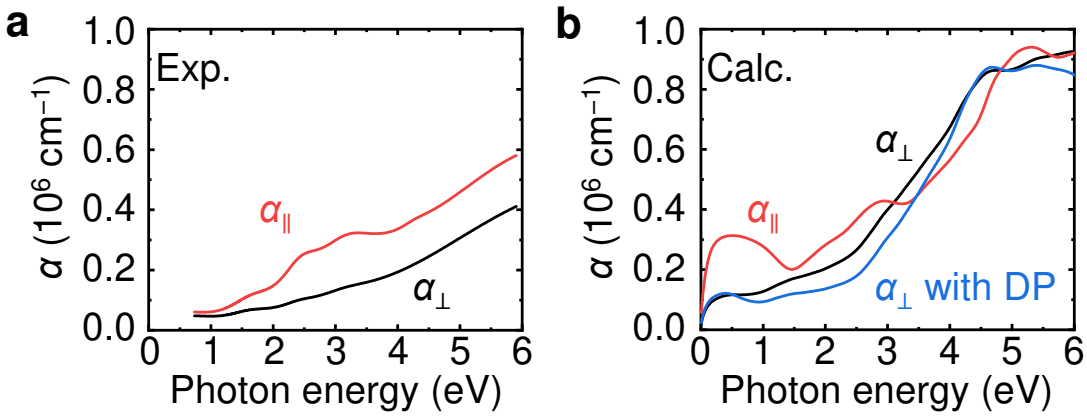

Figure 2. (a) Absorption coefficient spectra obtained from spectroscopic ellipsometry for light polarized parallel (red, $\alpha_\parallel$) and perpendicular (black, $\alpha_\perp$) to the nanowire axis. (b) Calculated absorption coefficients for the bulk crystal. The blue curve labeled "$\alpha_\perp$ with DP" represents the perpendicular absorption coefficients considering the depolarization (DP) effect.

Figure 2b shows the absorption spectra of a W_6Te_6 bulk crystal obtained from first-principles calculations. A broad absorption peak appears near 3 eV in the parallel direction ($\alpha_\parallel$), while the perpendicular absorption spectrum ($\alpha_\perp$) increases monotonically from 1 to 4 eV. This overall trend is consistent with experimental observations. However, above 3 eV, the calculated $\alpha_\perp$ slightly exceeds $\alpha_\parallel$, which contrasts with the experimental results.

To understand this discrepancy, we considered the depolarization effect. This effect is known to strongly influence the optical response along and perpendicular to the axis of carbon nanotubes.[26] When the depolarization effect is applied to the calculated $\alpha_\perp$, the anisotropy becomes more pronounced across most of the photon energy range, as shown in

Fig. 2b. Details of the calculations are provided in the Supplementary Material. In W_6Te_6 bundles, free carriers tend to screen the electric field of incident light when it is polarized perpendicular to the nanowire axis, thereby reducing the absorption in that direction. Since the bundle thickness in the perpendicular direction is typically on the order of 100 nm, much smaller than the optical wavelength, the electric field can be approximated as uniform across the cross-section. In contrast, for polarization parallel to the nanowire axis, the bundles are much longer than the wavelength of light, so the field remains unscreened. This directional difference in field screening leads to the strongly anisotropic optical response observed in these 1D nanowire systems.

The depolarization effect explains the suppression of perpendicular absorption in the visible range. Above 3 eV, however, our calculations for an ideal infinite crystal predict stronger absorption in the perpendicular direction than in the parallel one, which deviates from the experimental results. We attribute this discrepancy to the finite-size effect of bundles. For example, the finite bundle width (tens of nanometers) introduces numerous edges that enhance light scattering. This scattering may reduce the local internal field, particularly for the perpendicular polarization, and suppress the true absorption, as discussed for tubular structures of MoS_2.[27]

The differences between the experimental and calculated optical spectra also arise from the following factors. First, the bundles do not fully cover the substrate surface as shown in Fig. S1. This partial coverage may reduce the effective absorption coefficient α, refractive index n, and extinction coefficient κ. Second, the assumed height of the nanowire bundles affects the absolute values of the optical constants in the analysis (Fig. S2). Although a uniform thickness of 5 nm is assumed here, the fabrication of the uniform film remains future studies. We note that the bundles exhibit a root mean square roughness of about 2 nm (Fig. S1). In addition, while the calculations predict a pronounced peak around 4~5 eV, such a feature is not observed in the experimental spectra. Such discrepancies in peak positions may be attributed to the specific computational model used in the DFT calculations, temperature effects, or underestimation of the bandgap of W_6Te_6 bundles.

We also investigate the directional dependence in extinction (dichroism) and refraction (birefringence) obtained from optical model fitting of spectroscopic ellipsometry data. Figures 3a,b show the refractive index (n) and extinction coefficient (κ), respectively, in the

directions parallel ($n_{\parallel}$, $\kappa_{\parallel}$) and perpendicular ($n_{\perp}$, $\kappa_{\perp}$) to the nanowire axis. The parallel refractive index $n_{\parallel}$ exhibits peaks at 1.4 eV and 2.2 eV, and decreases beyond 2.2 eV. In contrast, $n_{\perp}$ shows no distinct peaks and gradually decreases with increasing photon energy. The extinction coefficient $\kappa_{\parallel}$ has pronounced peaks at 1.6 eV, 2.5 eV and 3.2 eV. In contrast, $\kappa_{\perp}$ increases monotonically above 2 eV with photon energy. The peaks observed in $n_{\parallel}$ and $\kappa_{\parallel}$can be attributed to interband electronic transitions, which will be compared with the calculated band structure later. In contrast, the suppression of $n_{\perp}$ and $\kappa_{\perp}$ can be ascribed to the depolarization effect, as discussed earlier. The increase in absorption below 1 eV is likely due to Drude absorption from free carriers. Figure 3c presents the birefringence ($\Delta n = n_{\parallel} - n_{\perp}$) and linear dichroism ($\Delta\kappa = \kappa_{\parallel} - \kappa_{\perp}$). Δn reaches ~0.5 in the 1–2 eV range, while $\Delta\kappa$ peaks at 0.6 around 2.5 eV.

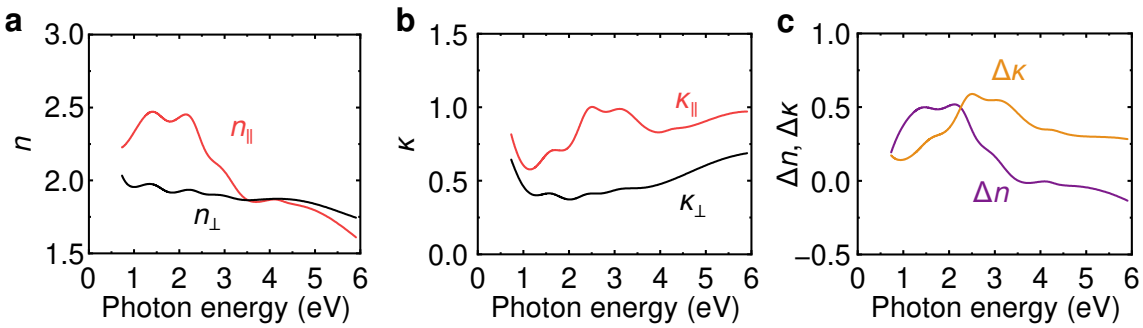

Figure 3. (a) Refractive indices ($n_{\parallel}$, $n_{\perp}$) and (b) extinction coefficients ($\kappa_{\parallel}$, $\kappa_{\perp}$) of aligned W_6Te_6 bundles obtained by ellipsometry measurements, where ∥ and ⊥ denote directions parallel and perpendicular to the nanowire axis, respectively. (c) Birefringence ($\Delta n = n_{\parallel} - n_{\perp}$) and dichroism ($\Delta\kappa = \kappa_{\parallel} - \kappa_{\perp}$), derived from the data in panels (a) and (b).

The magnitude of the observed birefringence in aligned W_6Te_6 bundles is comparable to that reported for semiconducting quasi-1D materials, such as TiS_3 (Δn = 0.3 at 560 nm),[2] ZrS_3 (Δn = 0.76 at 500 nm),[3] and fibrous red phosphorus (Δn = 0.642 at 475 nm).[4] However, unlike these semiconductors, W_6Te_6 is metallic, and its anisotropic optical response arises from delocalized charge carriers and a quasi-1D metallic band structure. This feature is expected to become even more pronounced in the infrared regime, as shown in Fig. 2b, which remains an open topic for future investigation.

Finally, to identify the origin of the absorption peaks, we investigate the electronic band structure, density of states (DOS), and joint density of states (JDOS) of the W_6Te_6 bulk crystal using first-principles calculations. Figure 4a shows the band structure, confirming the metallic nature of W_6Te_6 bulk crystal.[14,16,17] As shown in Fig. 4b, the DOS exhibits several sharp peaks, which correspond to Van Hove singularities arising from the quasi-1D structure of W_6Te_6. The transition of an electron from the Van Hove singularity at -0.5 eV to 2.0 eV and from -0.5 to 3.0 eV, which are indicated by the vertical arrows, can be assigned to the interband transitions of the observed absorption peaks in $\alpha_{\parallel}$ at ~2.4 eV and ~3.3 eV (see Fig. 2a), respectively. These transitions are likely attributed to excitations from Te *p*/W *d* hybridized valence bands to W *d* conduction bands.[22] We note that, in Fig. 4c, the 2.5 eV transition (orange circle) does not display a clear peak in JDOS because there are multiple energy dispersions in Fig. 4a for the orange solid circle in both the valence and conduction bands. On the other hand, the 3.5 eV JDOS peak is clear due to the larger Van Hove singularity at 3.0 eV in DOS as shown in Fig. 4b. We further note that the experimental absorption peak at 2.4 eV in Fig. 2a cannot be explained by JDOS alone. This suggests that the electron–photon interaction matrix elements play a significant role. It could also be questioned whether size effects contribute to the observed discrepancy. However, the present samples have an average thickness of around 5 nm, and by analogy with other van der Waals metallic systems, such as $NbSe_2$,[28] this thickness is expected to exhibit electronic states close to those of the bulk. For a more quantitative understanding, future studies involving orbital-resolved methods and excitonic effects will be necessary.

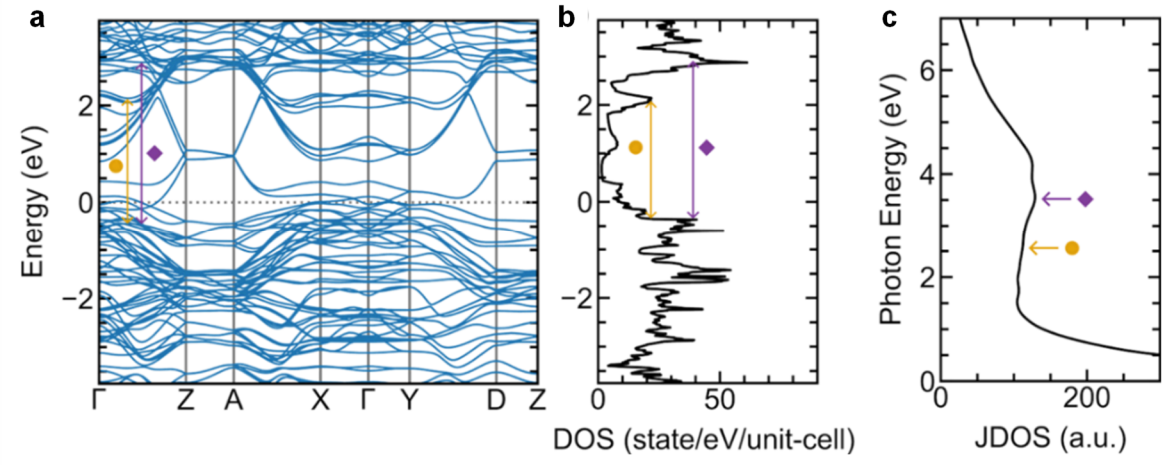

Figure 4. (a) Electronic band structure of W_6Te_6 bulk crystal along high-symmetry paths in

the Brillouin zone. (b) Total density of states (DOS) and (c) joint density of states (JDOS) of W_6Te_6 bulk crystal as a function of photon energy. The orange circle and purple diamond indicate representative optical transitions considered in the analysis.

In conclusion, we have investigated the optical properties of aligned W_6Te_6 nanowire bundles using a combination of spectroscopic ellipsometry and first-principles calculations. The results reveal pronounced anisotropic optical absorption and refraction, stemming from the quasi-1D structure of the nanowire bundles. The depolarization effect is introduced as a mechanism that suppresses absorption in the direction perpendicular to the nanowire axis, thereby enhancing the observed optical anisotropy. These findings provide valuable insights into light–matter interactions in quasi-1D metallic systems and highlight the potential of TMM nanowires for photonic and optoelectronic applications.

SUPPLEMENTARY MATERIAL

See the supplementary material for the detailed sample preparation, characterization, ellipsometry measurement and analysis, AFM images of aligned nanowire bundles, optical constant obtained by assuming different film thicknesses.

Acknowledgments

The authors acknowledge Ryuichi Koike for his support with the ellipsometry measurements. This work was supported by JSPS KAKENHI (Grant Nos. JP24KJ1874, JP21H05232, JP21H05234, JP22H00283, JP24H00044), JST FOREST (Grant No. JPMJFR213X), and the World Premier International Research Center Initiative (WPI), MEXT, Japan. R.S. acknowledges the support from the Yushan Fellow Program by the Ministry of Education (MOE), Taiwan. H.L.L. thanks the National Science and Technology Council of the Republic of China for its financial support under Grant No. NSTC 113-2112-M-003-002.

Conflict of interest

The authors declare that they have no conflicts of interest.

Data availability

Data supporting the results of this study are available from the corresponding author.

References

[1] S. Niu, G. Joe, H. Zhao, Y. Zhou, T. Orvis, H. Huyan, J. Salman, K. Mahalingam, B. Urwin, J. Wu, Y. Liu, T. E. Tiwald, S. B. Cronin, B. M. Howe, M. Mecklenburg, R. Haiges, D. J. Singh, H. Wang, M. A. Kats, and J. Ravichandran, Nat. Photon. **12**, 392 (2018).

[2] N. Papadopoulos, R. Frisenda, R. Biele, E. Flores, J. R. Ares, C. Sánchez, H. S. J. van der Zant, I. J. Ferrer, R. D'Agosta, and A. Castellanos-Gomez, Nanoscale **10**, 12424 (2018).

[3] S. Hou, Z. Guo, J. Yang, Y.-Y. Liu, W. Shen, C. Hu, S. Liu, H. Gu, and Z. Wei, Small **17**, 2100457 (2021).

[4] W. Chen, B. Zhang, K. Tao, Q. Li, J.-L. Sun, and Q. Yan, Angew Chem. Int. Ed. **63**, e202403531 (2024).

[5] B. Zhao, H. Mei, Z. Du, S. Singh, T. Chang, J. Li, B. Ilyas, Q. Song, T.-R. Liu, Y.-T. Shao, R. Comin, N. Gedik, N. S. Settineri, S. J. Teat, Y.-S. Chen, S. B. Cronin, M. A. Kats, and J. Ravichandran, Adv. Opt. Mater. **12**, 2400327 (2024).

[6] J. Lin, O. Cretu, W. Zhou, K. Suenaga, D. Prasai, K. I. Bolotin, N. T. Cuong, M. Otani, S. Okada, and A. R. Lupini, Nat. Nanotechnol. **9**, 436 (2014).

[7] J. Kibsgaard, A. Tuxen, M. Levisen, E. Lægsgaard, S. Gemming, G. Seifert, J. V. Lauritsen, and F. Besenbacher, Nano Lett. **8**, 3928 (2008).

[8] I. Popov, S. Gemming, S. Okano, N. Ranjan, and G. Seifert, Nano Lett. **8**, 4093 (2008).

[9] H. Zhu, Q. Wang, C. Zhang, R. Addou, K. Cho, R. M. Wallace, and M. J. Kim, Adv. Mater. **29**, 1606264 (2017).

[10] M. Nagata, S. Shukla, Y. Nakanishi, Z. Liu, Y.-C. Lin, T. Shiga, Y. Nakamura, T. Koyama, H. Kishida, and T. Inoue, Nano Lett. **19**, 4845 (2019).

[11] N. Kanda, Y. Nakanishi, D. Liu, Z. Liu, T. Inoue, Y. Miyata, D. Tománek, and H. Shinohara, Nanoscale **12**, 17185 (2020).

[12] Y. Xia, B. Wang, J. Zhang, Y. Jin, H. Tian, W. Ho, H. Xu, C. Jin, and M. Xie, Nano Lett. **20**, 2094 (2020).

[13] Y. Yoo, J. S. Jeong, R. Ma, S. J. Koester, and J. E. Johns, Chem. Mater. **32**, 9650 (2020).

[14] H. E. Lim, Y. Nakanishi, Z. Liu, J. Pu, M. Maruyama, T. Endo, C. Ando, H. Shimizu,

K. Yanagi, S. Okada, T. Takenobu, and Y. Miyata, Nano Lett. **21**, 243 (2021).

[15] H. E. Lim, Z. Liu, J. Kim, J. Pu, H. Shimizu, T. Endo, Y. Nakanishi, T. Takenobu, and Y. Miyata, ACS Appl. Nano Mater. **5**, 1775 (2022).

[16] H. Shimizu, J. Pu, Z. Liu, H. E. Lim, M. Maruyama, Y. Nakanishi, S. Ito, I. Kikuchi, T. Endo, K. Yanagi, Y. Oshima, S. Okada, T. Takenobu, and Y. Miyata, ACS Appl. Nano Mater. **5**, 6277 (2022).

[17] R. Natsui, H. Shimizu, Y. Nakanishi, Z. Liu, A. Shimamura, N. T. Hung, Y.-C. Lin, T. Endo, J. Pu, I. Kikuchi, T. Takenobu, S. Okada, K. Suenaga, R. Saito, and Y. Miyata, ACS Nano **17**, 5561 (2023).

[18] K.-H. Jin and F. Liu, Nanoscale **12**, 14661 (2020).

[19] I. Vilfan, Eur. Phys. J. B **51**, 277 (2006).

[20] D. Le, D. Sun, W. Lu, M. Aminpour, C. Wang, Q. Ma, T. S. Rahman, and L. Bartels, Surf. Sci. **611**, 1 (2013).

[21] Q. Liu and A. Zunger, Phys. Rev. X **7**, 021019 (2017).

[22] Y. Zhao, H. Qu, J. Zhao, L. Kang, and S. Zhou, Nano Lett. **25**, 1108 (2025).

[23] J. Deng, D. Huo, Y. Bai, Y. Guo, Z. Pan, S. Lu, P. Cui, Z. Zhang, and C. Zhang, Nano Lett. **20**, 8866 (2020).

[24] J. Deng, D. Huo, Y. Bai, X. Lin, Z. Cheng, and C. Zhang, Nano Lett. **23**, 7831 (2023).

[25] J. N. Hilfiker, N. Hong, and S. Schoeche, Adv. Opt. Technol. **11**, 59 (2022).

[26] K.-i. Sasaki and Y. Tokura, Phys. Rev. Appl. **9**, 034018 (2018).

[27] Q. Qian, R. Zu, Q. Ji, G. S. Jung, K. Zhang, Y. Zhang, M. J. Buehler, J. Kong, V. Gopalan, and S. Huang, ACS Nano **14**, 13333 (2020).

[28] X. Xi, L. Zhao, Z. Wang, H. Berger, L. Forró, J. Shan, and K. F. Mak, Nat. Nanotechnol. **10**, 765 (2015).